Transactions on Engineering and Computing Sciences - Vol. 12, No. 3
Publication Date: June 25, 2024
DOI:10.14738/tecs.123.17139.
Alvarez, R., & Camacho, M. (2024). The N-S Extension of The Mexico Basin is Confirmed by Gravity Analysis. Transactions on Engineering and Computing Sciences, 12(3). 149-174.

The N-S Extension of The Mexico Basin is Confirmed by Gravity Analysis

R. Alvarez
ORCID: 0000-0002-2606-0904
Instituto de Investigaciones en Matemáticas Aplicadas y en Sistemas (IIMAS), Universidad Nacional Autónoma de México, Coyoacán CDMX 04510, Mexico

M. Camacho
ORCID: 0000-0002-3871-6843
Posgrado en Ciencias de la Tierra, Universidad Nacional Autónoma de México, Coyoacán CDMX 04510, Mexico

ABSTRACT

The Mexico Basin is in the eastern portion of the Trans-Mexican Volcanic Belt, where it is repeatedly affected by strong ground motions. Notwithstanding, the tectonic setting of this region is not adequately defined, and several efforts are underway to improve its characterization. Here we use a high-resolution (220 m), satellite-derived gravity data set to acquire the matching Bouguer anomaly, from which 3D inversions are performed at varying resolutions, to obtain density distributions to depths of up to 15 km. The gravity signature agrees with an N-S extensional process previously recognized, based on geological arguments. Two gravity saddle points are identified flanking a minimum in the S portion of the basin; immediately southward is located Sierra del Chichináutzin, which we interpret as resulting from the N-S extensional process. Two relevant, not previously reported gravity anomalies are identified: the Ajusco Gravity Anomaly (AGA) and the Central Gravity Anomaly (CGA), the former associated with Ajusco volcano, and the latter with the central portion of Mexico City. The AGA contains two polygenetic structures: Ajusco volcano and San Miguel volcano; given their proximity to the Mexico and Toluca basins, a detailed exploration of their density distributions is performed. A comparison is made with seismic results reported elsewhere, between density and seismic velocity, finding good matches to depths up to 10 km below sea level.

Keywords: Basin of Mexico, Geological extension, Satellite-derived gravity, Gravity saddle point, Bouguer anomaly, Density distribution.

INTRODUCTION

Mexico Basin (MB), also known as Mexico City Basin (MCB), located in the eastern portion of the Trans-Mexican Volcanic Belt (TMVB). Mexico City is the largest, most populated city in the country, with a population of over 20 million, it is also a heavily industrialized area. The city area is continuously affected by seismic events, some of which have induced strong damage to it, particularly the 1985 earthquake (M 8.1) originating SW of the city, in a location where the Cocos plate begins to subduct under the North American plate [1,2]. The more recent one,

known as the 2017 Puebla earthquake, it struck at 13:14 local time on 19 September 2017 with an estimated magnitude of 7.1 M_w. Despite the seismic and volcanic risks pending on the city, the characteristics of its tectonic setting have not been adequately defined, particularly from geophysical approaches. The present one attempts to describe such characteristics using gravity field analyses, to depths of ~15 km. Figure 1 is a location map of Mexico City and neighboring volcanic structures in the TMVB.

In previous research about the deep characteristics of the Mexico Basin [3-7]) the only gravity data available at the time was used; it was a ground gravity survey [8] restricted in size to the Mexico City area. In the present study, we use satellite-derived gravity data designated GGM+ [9], discussed ahead, which has much larger coverage and considerably more dense distribution than the previous data set; this results in a more regional and more precise gravity data set, which allows for the identification of extensional processes occurring in the area, among other procedures.

We first analyze the Bouguer anomaly in the area from a general viewpoint to highlight its characteristics, and then proceed to superpose geologic maps on it to identify cause-effect relationships. In this frame, we can associate volcanic formations with tectonic processes. Then, we proceed to perform 3D inversions of the gravity data in the Mexico City area and extract density cross-sections of pertinent locations, which allows for an analysis of the first 15 km below the surface.

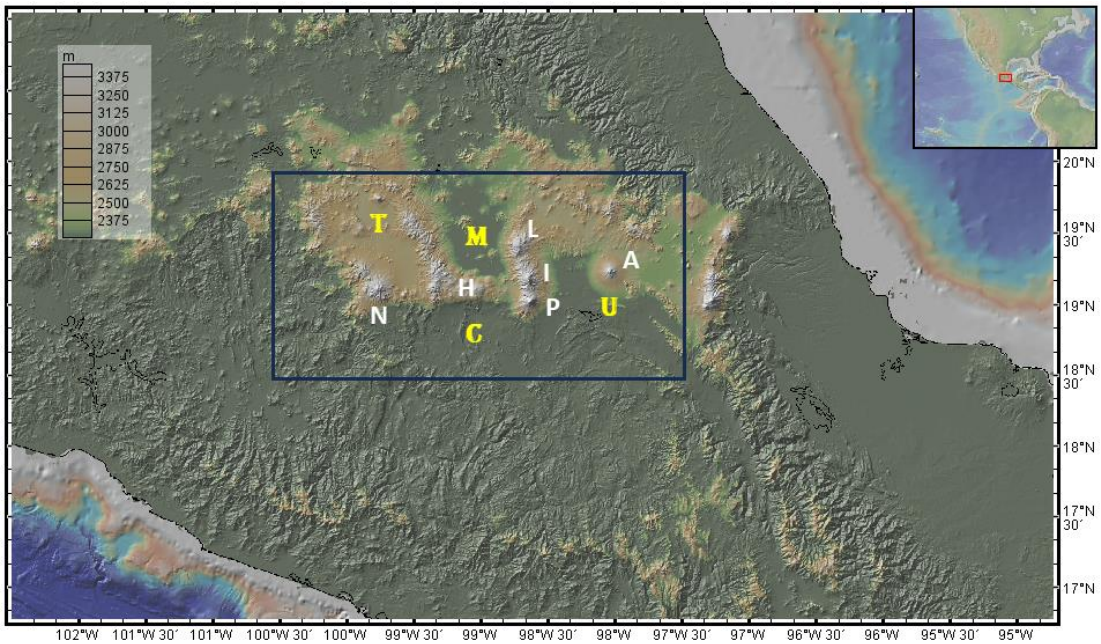


Fig. 1: Location map of the study area in central Mexico. Cities (yellow letters): T, Toluca. M, Mexico City, C, Cuernavaca. U, Puebla. Volcanic structures (white): N, Nevado de Toluca; H, Sierra Chichinautzin; P, Popocatépetl; I, Iztaccihuatl; L, Tláloc; A, Malinche. Sierra de Las Cruces trends NW, dividing Mexico (M) and Toluca (T) basins. DEM from GeomapApp [10]; http://www.geomapapp.org

GEOLOGY

Three tectonic events appear to have shaped the present Mexico Basin. The first one corresponds to the deposition of limestones and terrigenous rocks in the associated volcano-tectonic depression; its development started in the Cretaceous [11]. After the Laramide orogeny that occurred in the 80-35 Ma period, an E-W extension appeared to have increased the size and shape of the basin, subsequently filled by volcanic materials of the initial Trans-Mexican Volcanic Belt [12]. The second tectonic incident gave rise to the Mixhuca fault [13], inside the graben structure, and the formation of Sierra Las Cruces, which partially filled the graben. About 5 Ma, a new fault system began, trending SW-NE, associated with the Tenochtitlan mega shear [14]; these authors used the volcanic cones in the area, about 200 cones, to determine the local fracture distribution, identifying a NE-SW modern system of lateral displacement. They determined the azimuth of two or more monogenetic cones as the orientation of the main tectonic stress, parallel or subparallel to extensional shear fractures. In Sierra del Chichináutzin, south of Mexico City, they analyzed the relations between 132 cones, determining that orientation N55-75E tends to predominate over orientation E-W, and may be genetically related to faults in Sierra Las Cruces, Sierra de Guadalupe, and El Tezoyo, which have the same orientation.

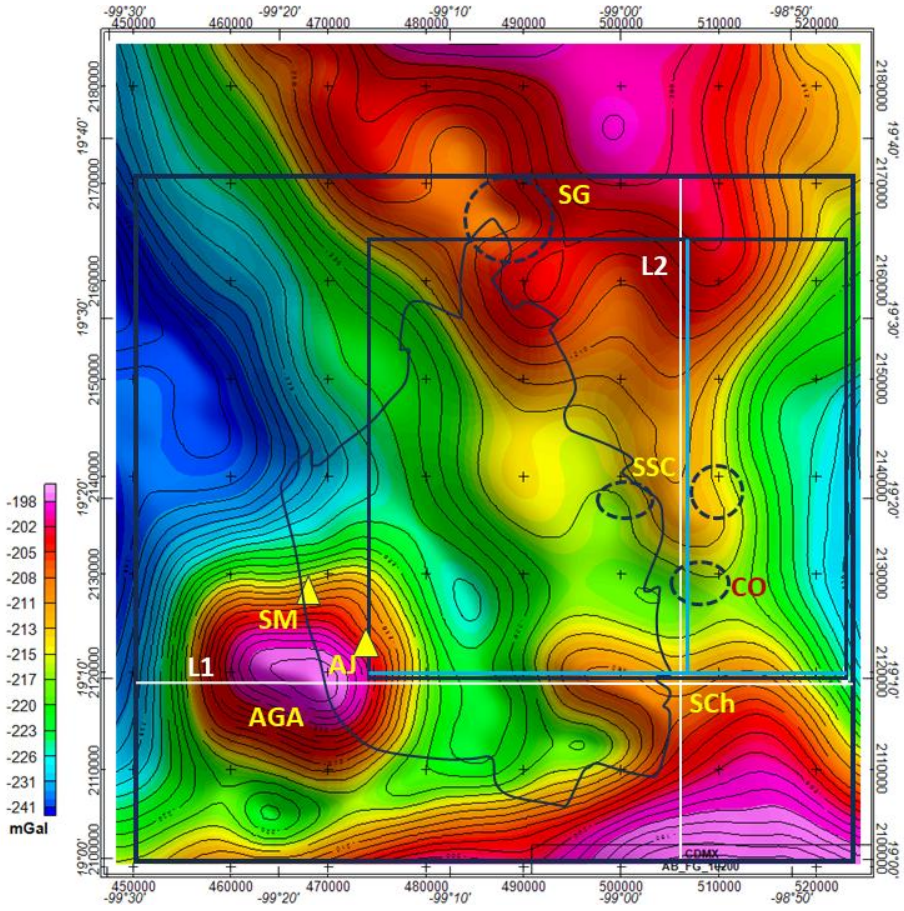


Fig. 2: Complete Bouguer anomaly map of the Mexico City area, detrended with a second-degree polynomial, from satellite-derived gravity data (GGM+); gravity values at ~220-m interval. The approximate location of the Mexico City area is outlined by the continuous black line. The large,

black rectangle indicates the region in which the 3D inversion at 2500 m resolution is performed; the smaller, black rectangle delimits the region in which the 3D inversion is performed at 1000 m resolution Two white lines (L1, L2) directed E-W and N-S show the location and extent of two cross-sections at 2500 m resolution, whilst the blue lines inside the smaller rectangle delimit the extent of the cross-sections at 1000 m resolution; they actually overlap the corresponding portions of white lines. Yellow triangles correspond to the Ajusco (AJ) and San Miguel (SM) volcanoes. AGA, Ajusco Gravity Anomaly. The region just N of Sierra Chichináutzin (SCh) exhibits a gravity low, to be analyzed below. CO, Chalco. SSC, Sierra Santa Catarina. SG, Sierra de Guadalupe.

About 20 monogenetic, volcanic cones are in the inner Mexico Basin [14] corresponding to Cerro El Peñón, Cerro de La Estrella, and the Chimalhuacán region, located over a fault inferred from gravimetry, oriented N50E. To the S there is the volcanic chain of Sierra Santa Catarina and Cerros de Cuetlapanca, Cocotitlán, and Xico, oriented N75-80E; these authors inferred that the Sierra de Santa Catarina alignment originated in a tensional fracture.

GRAVITY DISTRIBUTION

To the W, the Mexico Basin is flanked by Sierra de las Cruces, a Miocene-Pliocene formation of andesitic rocks [15] extending SE-NW from Sierra Chichinautzin, constituting a divide between the Toluca and Mexico basins (T and M in Figure 1). The large negative gravity anomalies to the E and W of the study area (Figure 2) correspond to young, active volcanic centers in which, among other volcanic structures, the outstanding edifices of Nevado de Toluca on the W side, and Iztaccihuátl, and Popocatépetl on the E side are located; the positive anomaly to the N holds Sierra de Guadalupe, a volcanic complex of domes of 14-15 Ma. To the S, the Quaternary, active field of monogenetic volcanoes that includes SCh [16-17], initiates a positive gravity trend terminating in the region of Cuernavaca City.

To the E of the Mexico Basin, there is the N-S alignment of Late Pleistocene-Quaternary volcanic structures: Tláloc, Iztaccihuatl and Popocatépetl (T-I-P); volcanic activity has migrated southwardly. This migration of the volcanic activity is quite similar to that observed in the western section of the Trans-Mexican Volcanic Belt, where Cántaro-Volcán de Nieve-Volcán de Fuego, in the Jalisco-Colima boundary, shows a trench ward migration of the volcanic activity [18]. There appears to be a fault-like boundary between Sierra Chichinautzin and the T-I-P volcanic sequence following an NNW-SSE direction, characterized on the surface by an accumulation of Quaternary volcaniclastic deposits and debris avalanches [19].

SADDLE POINTS

Traversing the map in Figure 2 along a NNW-SSE direction across the area of Mexico City we find a gravity decrement down to 19º-15’ and then it increases again. The opposite behavior is observed traversing the map in a W-E direction at that same latitude; that is, the gravity values increase reaching the Mexico City area and then decrease in the direction of the Popocatépetl and Iztaccíhuatl volcanoes, defining what appears as a gravimetric saddle point close to (98º 57’W, 19º 14’N), also known as a minimax point.

Figure 3 shows the region of the minimum, contoured to show in more detail its characteristics. The gravity minimum at (98º 55’W, 19º 15’N) divides the region of higher gravity values into

two sections, one to the N and the other to the S. To the E and W of this minimum, what appeared to be a saddle point, became two saddle (or minimax) points. Since gravity responds to mass concentrations, the minimum region indicates a mass deficiency in that location. The full gravity distribution suggests that the whole region with higher gravity values in the map has been extended in the N-S direction, a process that most likely continues to date. A supporting argument appears in [20], who reported generalized extensional conditions in the vicinity of the Mexico Basin, based on the existence of E-W vertical faults; they analyzed the southward migration of volcanism in the TMVB based on a two-layer crustal stretching process.

In Figure 3, the gravity maximum immediately S of the described gravity minimum is associated with Sierra Chichinautzin, a Late Pliocene-Quaternary, mafic and intermediate volcanic structure [19, 21] whose age is placed at 800-700 ka [22, 23]. Farther to the S of SCh there are abundant Quaternary volcaniclastic deposits younger than 40 Ka, and debris avalanches.

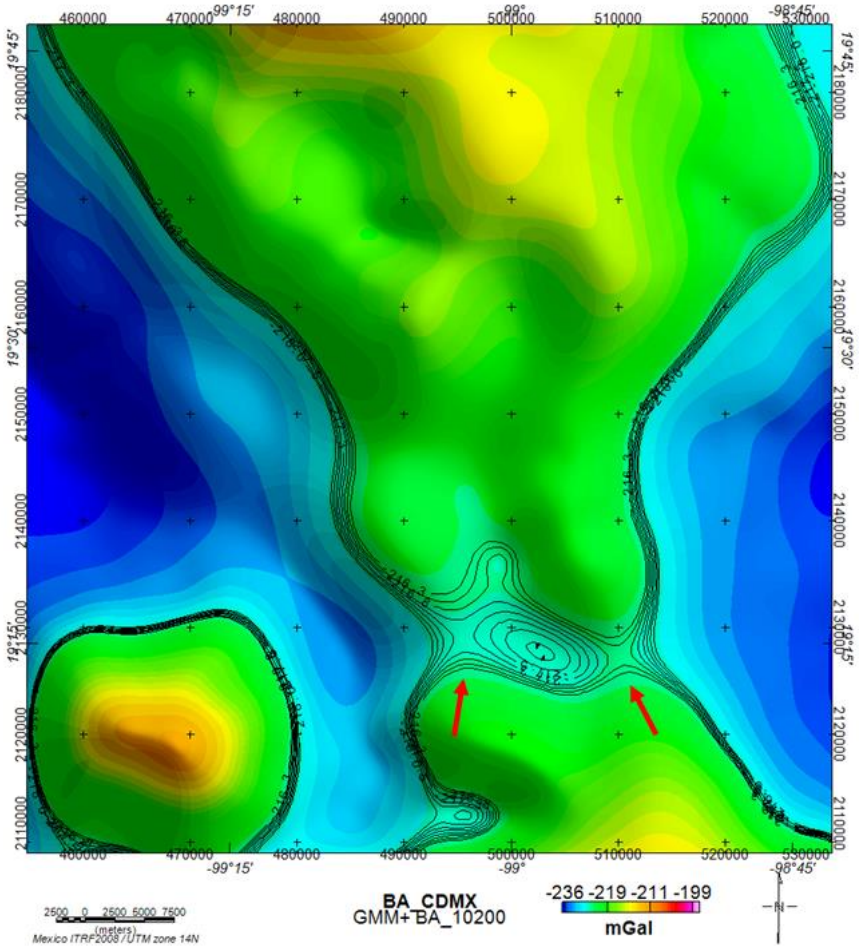


Fig. 3: A detailed contour display of the Bouguer anomaly map in Figure 2 enhances the characteristics of the minimax regions. The area corresponds to the full map in Figure 2. The minimum (98º 55'W, 19º 15'N) is flanked by two saddle points, indicated by arrows. The gravity contour interval is 0.25 mGal in a limited gravity range.

We submit that the recent formation of SCh is the result of this extensional process that has enabled numerous intrusions, as well as the presence of many monogenetic volcanic structures; the E-W orientation of the faults on SCh supports this assertion [11].

Furthermore, based on geochemical arguments [24] concluded that volcanism in SCh is mainly related to the upwelling of an anomalously hot mantle of the Ocean-Island-Basalt type, contrasting with the prevailing hypothesis proposing that the subducting Cocos plate is responsible for the origin of this magmatism, e.g., [25]. Additionally, the evolved magmas from SCh originated in the lower crust, from the partial melting of a heterogeneous mafic granulite magma source [26]. Considering that the upwelling mantle often induces extensional processes on the surface, e.g., [27], we conclude that this may be the origin of the observed gravimetric signature reported here. For correlation purposes, Figure 4 displays a composite image, where the Bouguer anomaly, the group of faults reported for the Basin of Mexico and its vicinity, as well as the geologic map of the region are superposed.

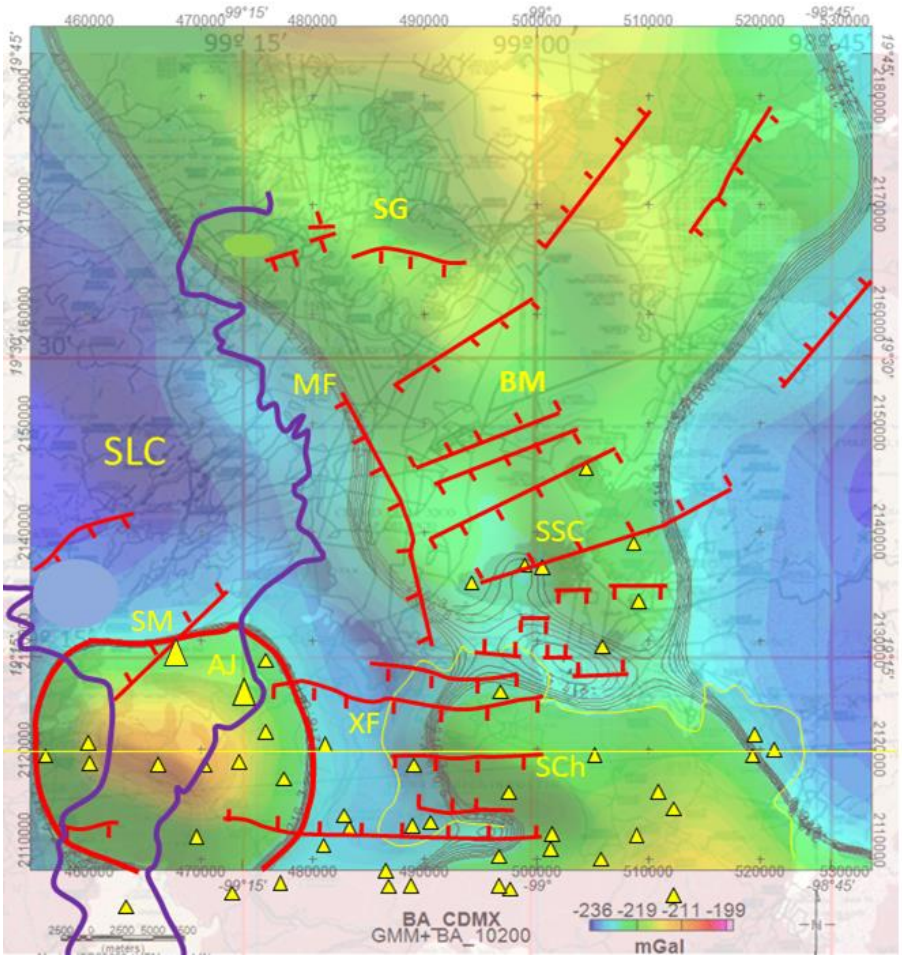


Fig. 4: For correlation purposes, we present the superposition of the corresponding portion of the Carta Geológico-Minera E14-2 (faint traces, SGM, 2002) of the Mexico City region on the Bouguer anomaly exhibited in Figure 3. Also superposed appear the geologic faults in the region, and the limits of Sierra de las Cruces (SLC, in blue, [11]). On the SW corner of the map, the gravity high (AGA) containing Ajusco volcano is also highlighted in red. San Miguel (SM)

volcano is located N of the gravity high. This superposition allows for a direct location of surface geologic features with the gravity anomaly; the alignment of faults with gravity features is remarkable, for instance, the Mixhuca fault tracks the gravity gradient in that region. Of particular interest is the gravity low located close to 99º 00', 19º 15', which is flanked E and W by two saddle points. A thin, yellow line exhibits the limit of SCh. The horizontal, yellow line at 2120000N corresponds to L1 in Figure 2. Small triangles represent monogenetic volcanoes. SLC, Sierra de Las Cruces; SM, San Miguel volcano; AJ, Ajusco volcano; SG, Sierra de Guadalupe; MF, Mixhuca fault; BM, Basin of Mexico; SSC, Sierra de Santa Catarina; XF, Xochimilco fault; SCh, Sierra Chichináutzin.

THE BASIN OF MEXICO

Immediately N of the reported gravity minimum is Sierra de Santa Catarina, represented by two, dashed ellipses (Figure 2), extending N75-80E, whose existence was attributed to an extensional process [14]. It is formed by the monogenetic, aligned volcanoes of Xaltepec, Tecuauhtzin, El Borrego, and Volcán La Caldera and the hills Yohualixqui, Tetecón, and La Estrella. These authors also report two sinking processes in the central portion of the basin, one occurring after the accumulation of the Tacubaya formation, and the second occurring between 10-7.5 Ka after the accumulation of the Becerra formation; they infer that faulting must have induced the sinking of the blocks. In [21] also concluded that the alignment of the monogenetic volcanoes in SCh is related to an N-S extensional regime, whose associated faults served as pathways for the eruption of these volcanoes. These processes correspond to a tectonically active region favoring the extensional characteristics of the province, as inferred from the gravity response.

These geochemical features, together with the geophysical and tectonic scenario of the Sierra Chichinautzin, indicate that volcanism in this area is mainly related to the upwelling of an anomalously hot OIB-like mantle [28, 29], and cast further doubts on a significant role of the subducting Cocos plate in the origin of this magmatism.

MB TOPOGRAPHIC CHARACTERISTICS

Figure 5 displays the DEM of the central portion of Mexico, where the MB is included; it shows that the MB is ~300 m below the neighboring plains to the E and W. From the characteristics of the gravity response, the elevation difference between the MB and the neighboring regions is attributed to a sinking progression of the MB induced by the extensional process inferred above.

An additional argument against this deformation originating in the subduction of the Cocos plate is provided by the distribution of seismic hypocenters. Some epicentral locations of earthquakes in the region are included to stress the difference between seismic activity originating in the subduction process, and seismicity originating in local faults and volcanic processes. The epicentral distribution tracks the subduction of the Cocos plate on this portion of Mexico: green epicentral locations close to the subduction region of the Cocos plate have depths <50 km, while the yellow ones have depths between 50 and 250 km; in the period analyzed, there is none registered under the MB. The red dots depict epicenters of Mg<4, usually shallow (<10 km) and associated with volcanism and geologic faults. As shown, this type of seismicity is present in and around Mexico's Basin.

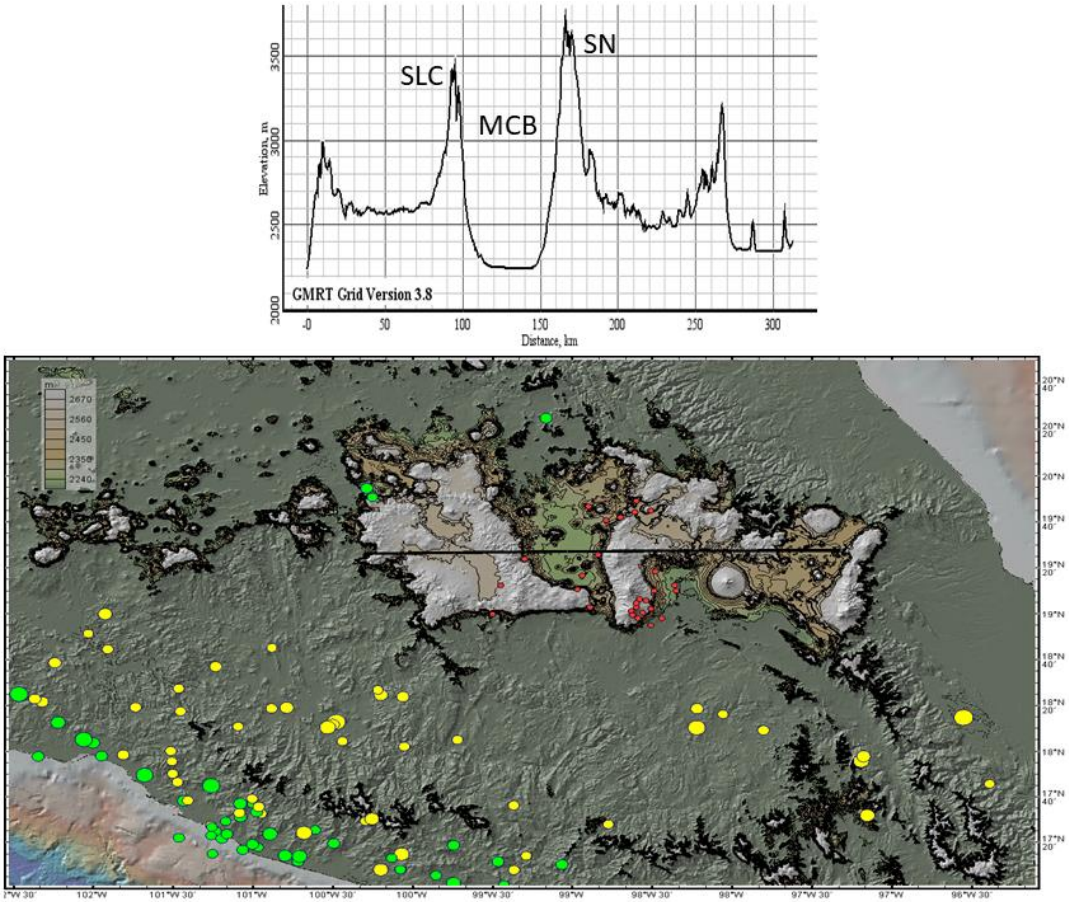


Fig. 5: a) 300-km topographic profile along the E-W, black line traversing the highlands region, showing it is above 2000-m elevation. The elevation of the Mexico Basin (MB) is ~300 m below the altitude of the neighboring regions. b) Topographic map from GeomapApp, GMRT Version 3.8); a group of volcano-dominated regions appear as light-colored areas in a portion of the Trans Mexican Volcanic Belt; they are above the 2000-m elevation. The MB shows as the light-green region in the middle of the E-W, black line across this region. Colored circles represent seismic epicenters from the International Seismological Centre, 1964-1995; Mg=5-9: Green, d<50 km; Yellow 50<d<250 km. From Servicio Sismológico Mexicano (1900-2021): red, Mg<4. SLC, Sierra Las Cruces. SN, Sierra Nevada.

3D INVERSION OF THE BA

Briefly explained the 3D gravity inversions are obtained using the method described in [30] based on the theoretical considerations exposed in [31]. The code was implemented in the Oasis Montaj program of Geosoft. The program uses a Cartesian Cut Cell algorithm (CCC) to represent geologic volumes and an Iterative Reweighting Inversion algorithm (IRI, [32]) to match the observed results with the calculated ones within established error limits, which in these cases is 5% of the standard deviation. The 3D inversion transforms gravity values (in mGal) to density values (in g/cm3); the depth of the inverted volume is proportional to the size of the volume selected for the calculation. Typically, choosing cubes of 500-m-long edges will attain depths of 5-6 km and greater depths can be obtained at the expense of the resolution. To optimize computation, a subset of the high-resolution data set is used, selected according to the model

resolution, to perform the inversion. The gravity inversion procedure is described in detail in [33-36]; the reader is referred to those publications for a complete description of the process.

Two rectangles in Figure 2 are selected for 3D inversion, both contain lines (L1, L2) or portions thereof, indicating where cross-sections of the inverted volume are obtained. The larger rectangle contains all of the Mexico City area, from which cross-sections will be obtained at a resolution of 2500 m. From the smaller rectangle, we obtain the 1000 m resolution inverted volume, to allow for more detailed analyses of the density distributions. Figure 6 shows the inverted volume of the larger rectangle at the 2500 m resolution.

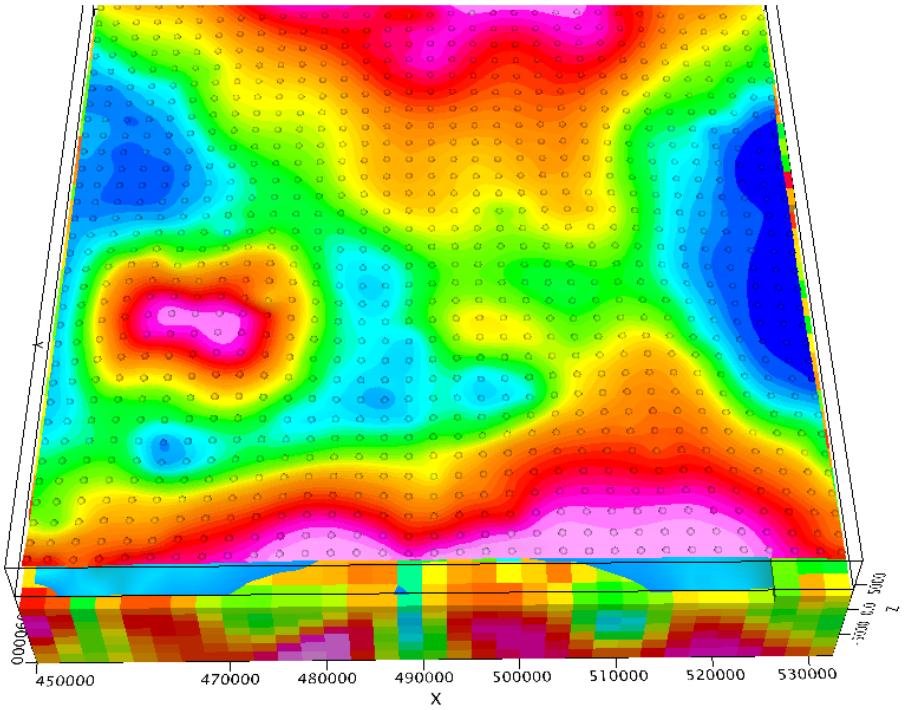


Fig. 6: Density model (3D) of the inverted Bouguer Anomaly shown in Figures 2, 3, and 4. For correlation purposes, the gravity produced by the density distribution of the model, and the uniform distribution of gravity stations (circles) are displayed. Underneath appears visible a portion of the inverted volume; the model resolution is 2500 m and the depth reached is 10 km bsl. The accompanying Digital Elevation Model (DEM) is not displayed to avoid overcrowding. Cross-sections will be extracted from this volume to analyze specific regions.

INVERSIONS AT 2500M AND 1000M RESOLUTION

3D inversions were performed, and several cross-sections extracted from them will be compared in this section. The difference in resolution contributes to a more complete understanding of the density dispersals. In Figure 2, two rectangles delimit the areas in which the Bouguer Anomaly is inverted; one has a model resolution of 2500 m, and the smaller one of 1000 m resolution. Two, perpendicular yellow lines (L1, L2) indicate the position and extent of two cross-sections obtained at the 2500-m resolution, and two, blue lines within the smaller rectangle indicate the position of the corresponding cross-sections at 1000-m resolution. The two sets of cross-sections overlap where indicated.

In the discussions of the cross-sections obtained from the 3D inversions, we repeatedly use the high-density and low-density qualifiers. Since all cross-sections include a color scale, the actual values implied by low, and high, can be directly inferred from those scales. Generally, the low values are represented in blue and the high values are in red tones.

From the density model shown in Figure 6, we extracted the density cross-section in the W-E direction, as shown by the yellow line (L1) in Figure 2. L1 extends W to E, from the location of San Miguel volcano, through Ajusco volcano, the Xochimilco region, Sierra Chichináutzin, San Pablo Atlazalpa, and the low-density anomaly associated with the W portion of Iztaccihuatl volcano. The corresponding cross-section, extracted from the volume in Figure 6 is displayed in Figure 7a.

San Miguel and Ajusco volcanoes relate to the large, cone-shaped, high-density region that appeared in the SW portion of Figures 2-4, which we will refer to as the Ajusco Gravity Anomaly (AGA) since it is large and isolated. The cross-section (Figure 7a) shows a density maximum located at X=-20 km and Z=5-6 km bsl, with an extension to the W, outspreading its size in that direction. Thus, the high-density distribution generating the AGA is deeply rooted, extending below -10 km bsl (Figure 7a). Both polygenetic volcanoes have been dated between 2.3 and 0.4 Ma [37, 38], and a Plinian, recent eruption at 37-25 ka has been attributed to the Ajusco volcano [39].

From these observations, we derive a possible explanation for the existence of this large, isolated, high-density anomaly related to AGA, including San Miguel and Ajusco volcanoes: the N-S extensional process observed in the Basin of Mexico was already present at about 2.5 Ma, inducing magma injection of low density in the Ajusco region, creating a low-density section under it, with the center of the magma chamber located at Z=5-6 km bsl, feeding the corresponding volcanic edifice. Concurrently, or shortly after that, the material of the magma chamber displaced toward the W and upwards, inducing the eruptions of the San Miguel volcano. Subsequently, the whole magmatic distribution cooled off, becoming a high-density distribution as observed to date, leaving a few magma pockets, one of which reactivated in the Plinian eruption attributed to the Ajusco at 37-25 ka [39].

The AGA is separated from SCh by a deep, low-density channel that on the surface, and along this cross-section, corresponds to the Xochimilco Lake. The center of the low-density distribution appears to be at -10 km bsl. It shows a surficial deflection to the E slightly below sea level, forming a low-density pocket at the surface, apparently fed by the lower distribution. This region should be analyzed by means other than gravity, since it may be

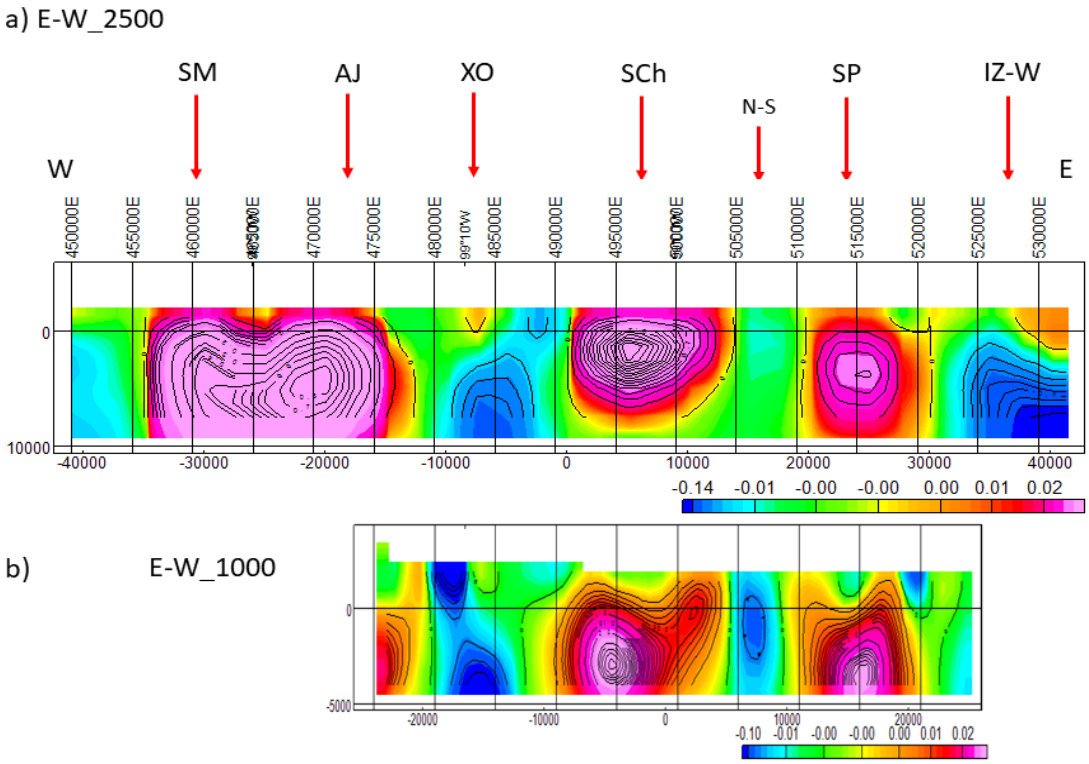


Fig. 7: a) Cross-section in the E-W direction extracted from the density distribution obtained after the 3D inversion (Figure 4) of 2500-m resolution. Its location is shown in Figure 2 by L1. b) Below, and aligned with L1, there is the corresponding, overlapping cross-section at 1000-m resolution; notice the more detailed definition of the anomalies and the subtle changes in density values. The changes in density limits (color scales) result from averaging density in a prism of 2500 m on the side, versus averaging density in a prism of 1000 m on the side. SM, San Miguel volcano. AJ, Ajusco volcano. XO, Xochimilco, SCh, Sierra del Chichináutzin. SP, San Pedro Atlazalpa. IZ-W, Iztaccihuatl Western Anomaly. N-S, intersection with the line in Figure 8. Density values are those of the color scale +2.67 g/cm3.

the location of intruded magmatic material, as observed in the neighboring regions of Ajusco and SCh. In [26] proposed that in this region, magmas inducing monogenetic volcanism ascend rapidly along E-W extensional faults, not having time to form large magma chambers. Magmas feeding the polygenetic volcanoes originate in a brittle-ductile transition zone in an upper crustal level and are maintained there for longer periods, forming large magma chambers, whose materials subsequently ascend along N-S to NNW trending faults.

Continuing to the E we find SCh, which is also a high-density distribution exhibiting a density maximum likely owing to dike injection [26]. There is an important difference between the high-density regions of AGA and SCh: while the former reaches the bottom of the model at 10 km bsl suggesting that it continues to deeper extents, the latter shows its bottom at 9 km bsl. SCh is considerably younger than Ajusco and San Miguel since its activity has been dated from 1.2 Ma [40] to as young as 1.6 ka [41, 42]. Before the existence of SCh, the drainage of the Mexico Basin was toward the S; after its expansion, the basin's drainage was closed [43, 44]. The build-up process of SCh has been attributed to the injection of dikes [26]. Given the proximity of

Ajusco and San Miguel volcanoes to SCh, it is surprising their different genetic nature; most likely, their different ages correspond to different extensional episodes of the crust, and thereby their variations.

East of SCh there is a wide, low-density region with a positive anomaly (SP) in the middle. As in the cases of AGA and SCh, SP shows a central maximum at 4 km bsl; its flanks are vertical and reach the bottom of the model, from which we infer that they are vertical faults bounding another region of intrusions. East of this region there is a low-density distribution, which is associated with the western, low-density anomaly of Iztaccíhuatl volcano.

Turning now to the 1000-m resolution inversion of a portion of L1 (Figure 7b), we observe that the corresponding density anomalies experienced changes in their geometries because of the improvement in the resolution; also, the model's depth decreased from 10 to 5 km. For instance, the SCh transformed into a high-density region with a maximum located at 495000E and -3 km depth, from which a branch extends to the E, reaching the surface. This would indicate that at some point there were, not one but two magma sources at the surface of SCh. One magma source is implied by the lower-resolution result in Figure 7a. In the case of the SP anomaly, a similar observation can be made. Although the higher resolution inversion does not reach the AGA, an analogous phenomenon would be exposed in that location.

Next, we analyze the N-S cross-section at a resolution of 2500 m which appears in Figure 8. The high-density anomaly of SCh shows that the center of the distribution is at -10 km bsl, contrasting with what was found in Figure 7. This indicates that this region is the main feeder of magmatic material to SCh, conveying such material upward and to the W to reach the distribution displayed in Figure 7.

Close to the center, this cross-section intersects Chalco Lake, a deep region of low-density materials that is also intercepted by the E-W cross-section in Figure 8b. Beyond this region, there is Sierra Santa Catarina, underlain by high-density material that extends and dips to the N, to the end of the cross-section. This high-density region under SSC shows a maximum at -5 km bsl, which also resembles an abandoned magma chamber. The density distribution registers the presence of SSC graben, and farther to the N the Basin of Mexico reaches a depth of 3 km under the surface, characterized by medium-density materials. The SSC graben is located (Figure 4) between two geologic faults separated between 6 and 8 km that correspond to the region designated GRA in Figures 8a and 8b; the upper area in the models (2140000N, green) shows the graben region reaching a depth of up to 3 km. The graben deposits are mostly Becerra and Tacubaya formations intermixed with sediments and volcanic debris [14].

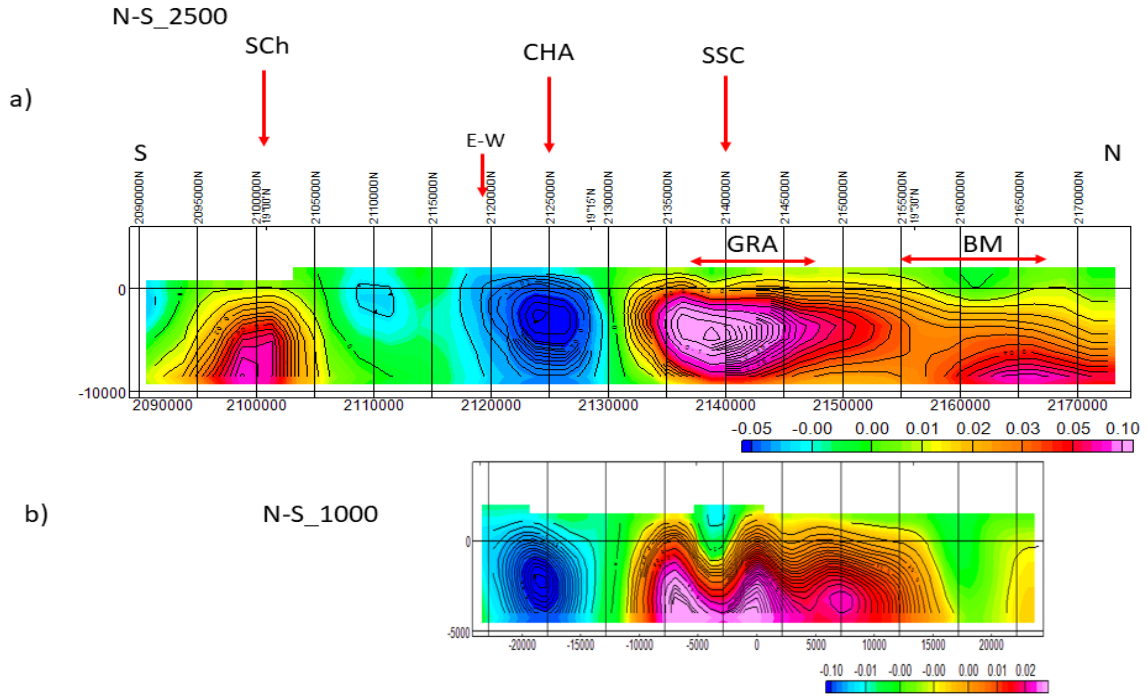


Fig. 8: a) Cross-section in the N-S direction extracted from the density distribution obtained from the 3D inversion (Figure 6). Irts location is shown in Figure 2 by the vertical, yellow line at 98º 57'W. b) Below, and aligned with L2, there is the corresponding, overlapping cross-section at 1000-m resolution; notice the more detailed definition of the anomalies and the subtle changes in density values. SCh, Sierra del Chichináutzin. CHA, Chalco. SSC, Sierra de Santa Catarina. GRA, SSC graben. BM, Basin of Mexico. E-W, intersection with the line in Figure 7. Density values are those of the color scale +2.67 g/cm3.

SAN MIGUEL AND AJUSCO VOLCANOES

In this section, we analyze in more detail two stratovolcanoes that may induce potentially disruptive events in the Mexico City and the Toluca City areas. The San Miguel and the Ajusco are two polygenetic volcanoes located SW of the Mexico Basin, whose ages have been reported between 2.3 and 0.4 Ma [37, 38]; they are associated with a prominent, circular region of high density, the Ajusco Gravity Anomaly (AGA, Figures 4 and 9), which is reported here for the first time. The AGA is crossed by Sierra de Las Cruces and Sierra del Chichináutzin; according to the geologic map reported in [39], both sierras overlap in this region of gravity high; these authors also report a fall deposit of pomez, called the Tlalpan Forest Pomez dated by radiocarbon between 25 and 37 ka, whose emission center was tentatively associated with the Ajusco volcano. They ruled out the volcanoes of SCh as a possible source since monogenetic volcanoes do not emit pomez, but rather scoria fragments of more basic composition. If this interpretation is correct, the Ajusco volcano has had a fairly recent reactivation, posing a potential risk to Mexico City and to the Toluca Basin to the W. The above reasons showed the pertinence of a detailed look at the characteristics of the AGA.

In Figure 9 a new rectangle enclosing the AGA is shown, defining the area where a new 3D gravity inversion is performed, and three density cross-sections (A1-A3) will be extracted. A new region designated the Central Gravity Anomaly (CGA) is also identified; it is characterized

by an anomalous decrement of gravity, contrasting with its immediate surroundings; remarkably, it overlaps with the region of major damage in the 1985 and 2017 earthquakes.

We note that the AGA and the high-gravity region of SCh are separated by a low-density channel running in the N-S direction between them. Furthermore, this channel presents a minimum, that an associated E-W extensional phenomenon might have induced, between Saddle Point W and the AGA. The volcanic activity of SCh crosses this region of minimum gravity as shown in Figure 4, ending at the W limit of the AGA region. From the corresponding 3D inversion, similar to the one displayed in Figure 6, the three density cross-sections (A1-A3) indicated in Figure 9, will now be discussed to understand better the deep-rooted characteristics of Ajusco (AJ) and San Miguel (SM) volcanoes.

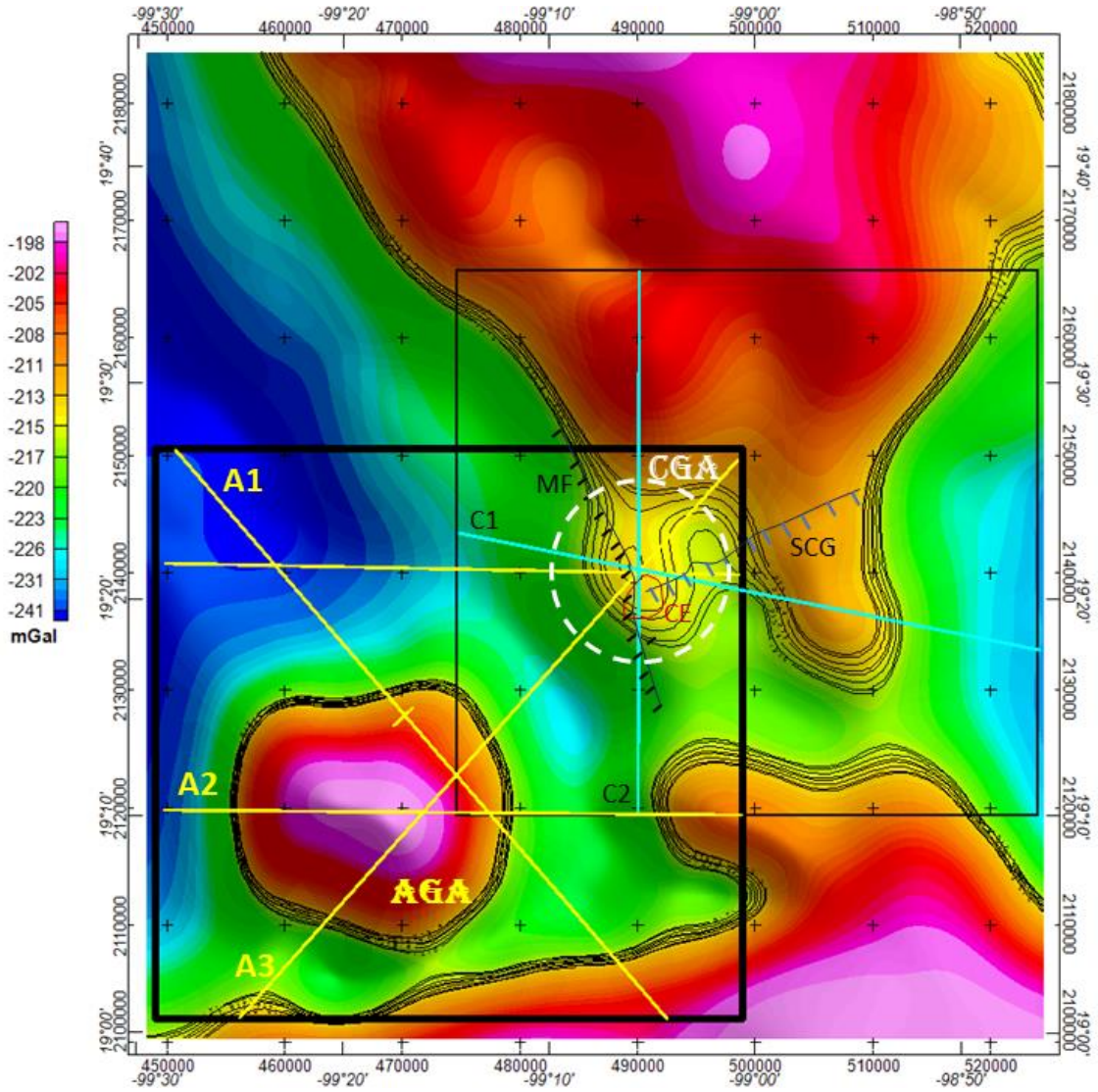


Fig. 9: On the Ajusco and San Miguel volcanoes region, an additional 3D inversion at 1000-m resolution was performed in the area enclosed by the black rectangle containing the large, isolated gravity anomaly on the SW portion (AGA). A1-A3 locate the cross-sections derived from this 3D inversion. Ajusco Volcano is located at the intersection between cross-sections A1

and A3, while San Miguel is located on the NW portion of A1 (small line crossing A1). CGA, Central Gravity Anomaly. MF, Mixhuca fault. SCG, Santa Catarina graben, CE, Cerro de La Estrella. The area of the Central Gravity Anomaly is indicated by a dashed circle. Blue lines correspond to cross-sections C1 and C2 obtained from the 3D inversion corresponding to the black rectangle enclosing them.

Density cross-section A1 extends 60 km from NW to SE, intersecting SM and AJ structures. Figure 10 shows that the density cross-section reaches 5 km bsl; it also indicates the locations of SM and AJ volcanoes, and the low-density regions (LD). What appeared to be a solid mass of high-density material in the 2500-m resolution version (Figure 7, SM, AJ) looks now like a region where high- and low-density regions alternate in its upper portion. This is a direct consequence of using a higher resolution in the 3D inversion since it averages density in smaller volumes. At the 1000-m resolution, A1 displays three sections with high-density distributions, two of them enclose a lower-density channel that reaches the surface, coinciding with the location of SM volcano; also, AJ shows regions of lower density associated with it, within sea level and the surface, the low-density pockets are usually associated with deposits that may induce volcanic activity, such as monogenetic cones or the pomez ejecta attributed to AJ. The low-density channel (LD) on the SE portion of A1 indicates the potential existence of a magma deposit centered below -5 km, with a branch to the SE centered at -2 km, the latter can be considered an active part of SCh given the existence of several monogenetic cones on the surface (Figure 4).

We note that the AGA region (SM and AJ) and the LD region (Figure 10) both show density sections that have a maximum or a minimum at 5 km bsl; given their similar geometric appearance and the abundance of volcanic phenomena in this region, we infer that the high-density distributions were initially low-density, high-temperature ones, whose feeding was eventually canceled, subsequently cooling and solidifying but maintaining the initial magmatic pattern. Similar results about high-density distributions associated with volcanism have been recently reported in the case of Tancítaro and Paricutín volcanoes [45]. The region corresponding to Pelado Volcano also displays a minimum at -5 km bsl, showing a low-density, vertical section from sea level to the terrain surface, corresponding to the volcano located at (485000W, 2110000N) in Figure 4; it also displays a bifurcation toward the SE, creating a surficial, low-density pocket. The three centers of low- and high-density distributions (LD, SM-AJ, PE) found along Line A1 lead us to assume that the -5 km depth is favored for the concentration of magmatic deposits in the AGA.

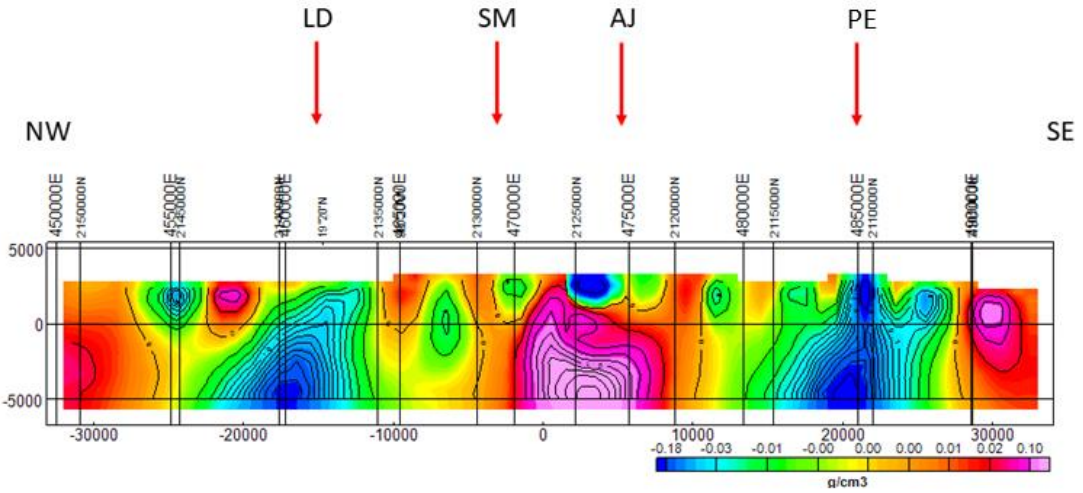


Fig. 10: Density cross-section along line A1 (Figure 9). LD, low-density region. SM, San Miguel Volcano. AJ, Ajusco Volcano. PE, Pelado Volcano. The color scale shows density values +2.67 g/cm3.

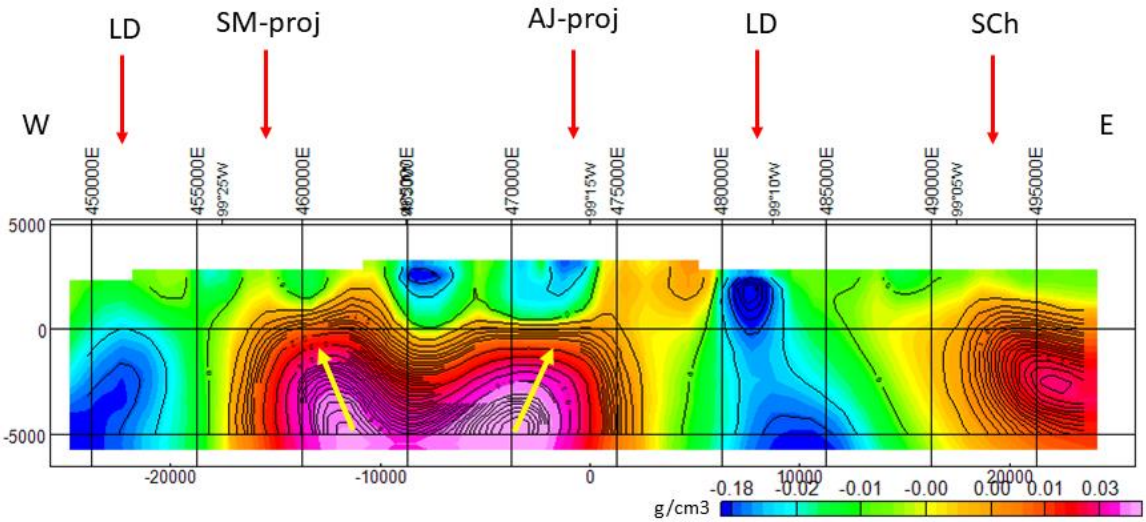


Fig 11: Density cross-section along line A2 (Figure 9). The yellow arrows indicate possible flow paths in the past. Proj indicates projected locations. LD, low-density region. SCh, Sierra Chichináutzin. The color scale shows density values +2.67 g/cm3.

Density cross-section A2 extends 50 km from W to E, intersecting LD in two portions, which enclose the high-density distribution corresponding to the AGA. The projected locations of SM and AJ and the high-density anomaly of SCh to the E are indicated. The density region corresponding to the AGA displays low densities in the upper 4 km, correlating with the observations made along A1. Two arrows indicate trajectories towards the surface that correlate with the directions of SM and AJ, indicating that these are effectively two lobes extending from A1 to this position. The E, LD region shows another coincidence of a low-density region reaching the surface, with the presence of a monogenetic volcano located at (480,000, 2120000) in Figure 4.

Density cross-section A3 extends 60 km from SW to NE, intersecting LD in two portions, SW and NE, which enclose the high-density distribution corresponding to the AGA. This cross-section intersects AJ volcano, within the high-density region. The center of the high-density distribution is located at -5 km elevation; it exhibits an NE branch (yellow arrow) that is apparently the remains of the magma conduit feeding directly to Ajusco volcano. The surficial, low-density pockets observed in cross-sections A1 and A2 are less conspicuous here. The LD zones have approximate surface extents of 8-10 km and circular density distributions with centers, LD-SW at 1 km asl, and LD-NE at 3 km bsl. The center location of the high-density region containing the Ajusco anomaly is also circular, displaying a maximum at 5 km bsl. The Central Gravity Anomaly (CGA) is circular, with a center at -4 km bsl. Notice the various density gradients within these distributions.

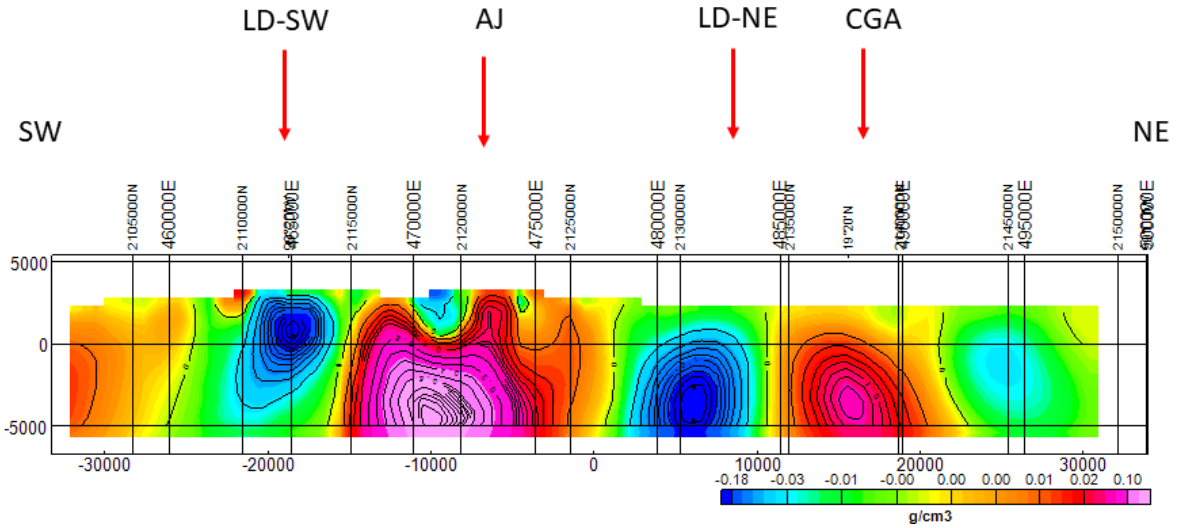


Fig. 12: Density cross-section along line A3 (Figure 9). AJ, Ajusco volcano. LD-SW, Low-density SW. LD-NE, Low-density NE. CGA, Central Gravity Anomaly. The color scale shows density values +2.67 g/cm3.

The analysis of the AGA with the 1000-m resolution inversion indicates that it was generated by two, similar, high-density masses, which appear to have been placed as low-density distributions, as inferred from their present geometric dispersals, experiencing a cooling process that transformed low-density regions into high-density ones. The two masses start separating at an elevation of ~2 km bsl, reaching the surface, one at the location of San Miguel volcano, and the other at Ajusco volcano. Figure 13 displays a horizontal section of the 3D inversion performed on the rectangle enclosing the AGA (Figure 9) at a depth of 1840 mbsl, where the anomaly bifurcation is obvious.

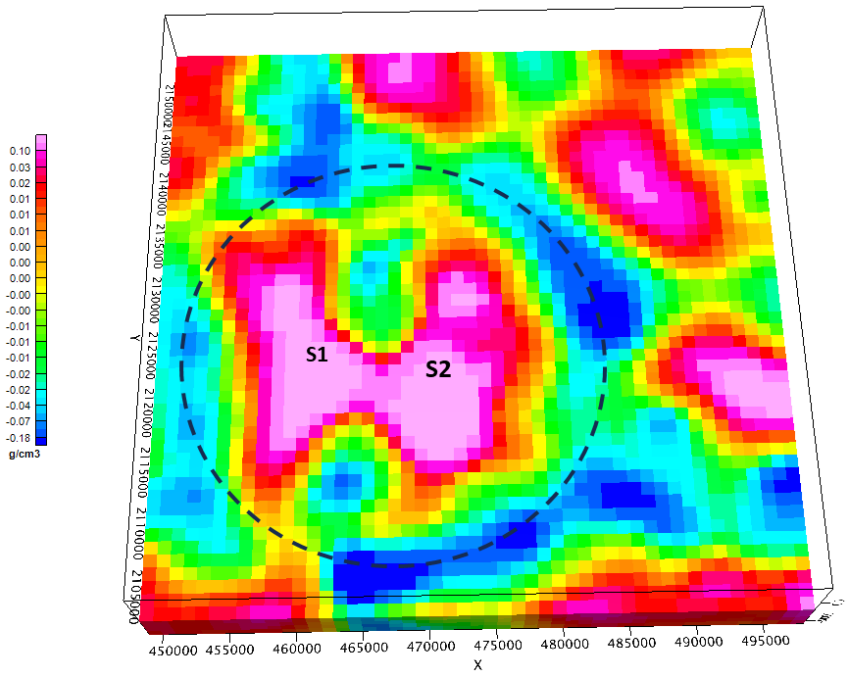


Fig. 13: Horizontal section at 1840 mbsl, showing the two sections S1 and S2 in which the density distribution corresponding to the AGA is split. S1 would feed San Miguel volcano and S2 would feed Ajusco volcano. The dashed circle joins the low-density regions that surround S1 and S2 to that depth. The color scale shows density values +2.67 g/cm3.

THE CGA

The region occupying the Central Gravity Anomaly appears in Figure 9; it has a gravity of intermediate values that calls attention since it differs from the higher gravity values surrounding this region on the N, S, and E sides. Two blue lines in the map of Figure 9 show the location of cross-sections C1 and C2. The gravity high in the N portion of the map bifurcates into two lobes before approaching the gravity minimum to the S. The W-lobe constitutes the CGA; the E-lobe and the surrounding regions display higher gravity values, making the CGA an anomalous region. The CGA also shows a close relation to the damaged areas in Mexico City in the 1985 and 1917 earthquakes, increasing the significance of this region; it also coincides with the lowest topographic region in the W portion of the Mexico Basin.

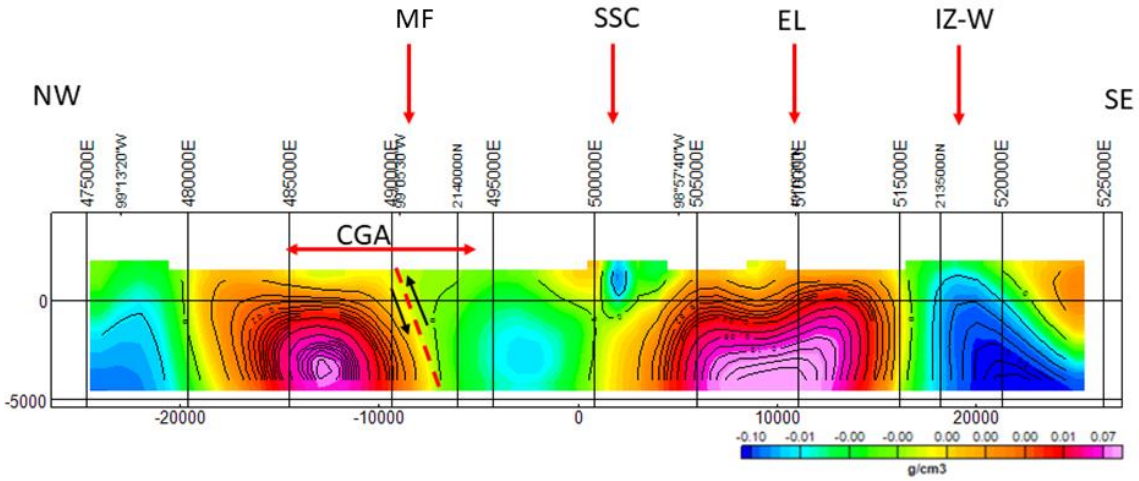


Fig. 14: Density cross-section along C1 (Figure 9) across the CGA at 1000 m resolution. Mixhuca Fault (MF) is inferred at the high-density-low-density contact; the arrows indicate the relative motions along the fault plane. SSC, Sierra Santa Catarina. EL, Eastern lobe. IZ-W corresponds to the W portion of the Iztaccíhuatl low-density anomaly. The color scale shows density values +2.67 g/cm3.

Figure 14 displays the C1 (NW-SE), density cross-section across the CGA at a resolution of 1000 m. The lower density values of the CGA, to those of the Eastern Lobe, can be easily appreciated. Mixhuca fault is located along the contact between the indicated high- and low-density regions. Sierra Santa Catarina presents a mixture of medium- and low-density values.

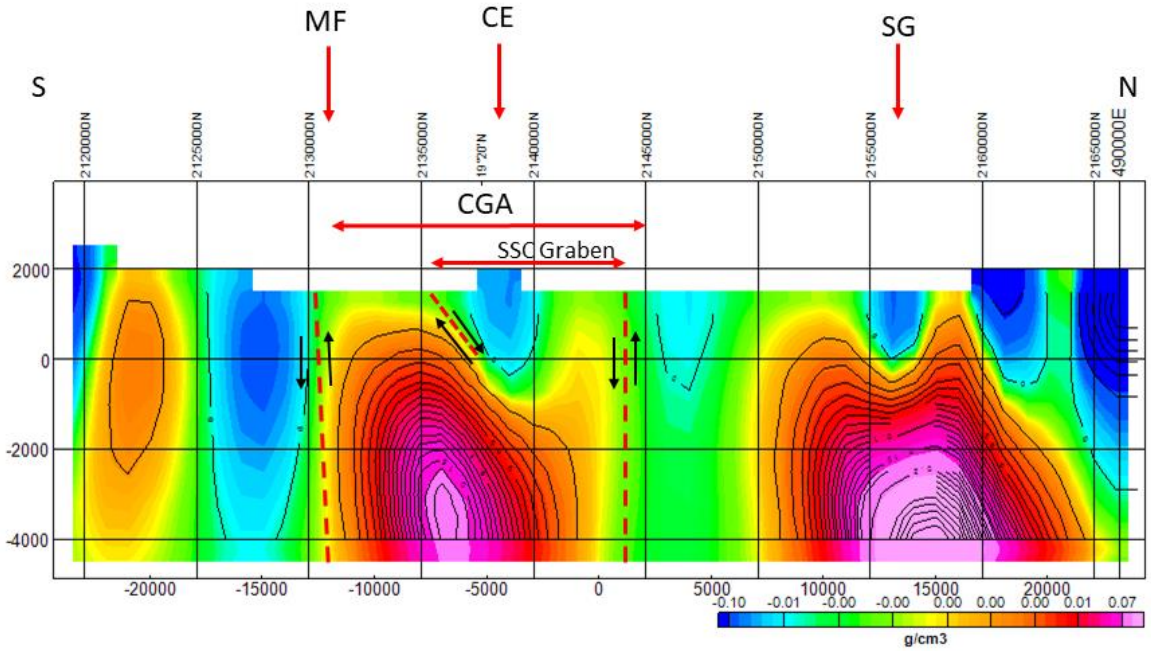


Fig. 15: Density cross-section along C2 (Figure 9) across the CGA, at 1000 m resolution. MF, Mixhuca fault. CE, Cerro de la Estrella. SSC, Sierra Santa Catarina graben. SG, Sierra de Guadalupe. The color scale shows density values +2.67 g/cm3.

Figure 15 displays the C2 (N-S), density cross-section across the CGA at a resolution of 1000 m. Mixhuca fault is located along the contact between the high- and low-density regions indicated. The high-density region, next to the N, contains a significant notch of low-density that corresponds with Sierra Santa Catarina graben. The volcanic structure at its center corresponds to Cerro de La Estrella. Sierra de Guadalupe (SG) is located farther to the N; notice again the larger size of the SG anomaly about that of CGA. The low-density regions within, and N of Sierra de Guadalupe appear to be linked to geologic faults.

CRUSTAL STRUCTURE

Seismologists have described the crustal structure under the Mexico Basin [46, 47]; we will compare some of our results with the most recent seismic work available [48], which uses and inverts velocity and acceleration records (i.e., receiver functions) and dispersion curves. The best resolution they report is 7.5 km, which is from 3 to 7.5 times the resolution of our models; however, they mostly use a resolution of 15 km, considered optimum by them since it allows interpretations within the limits of their study area. Despite the large resolution differences, some general correlations can be established.

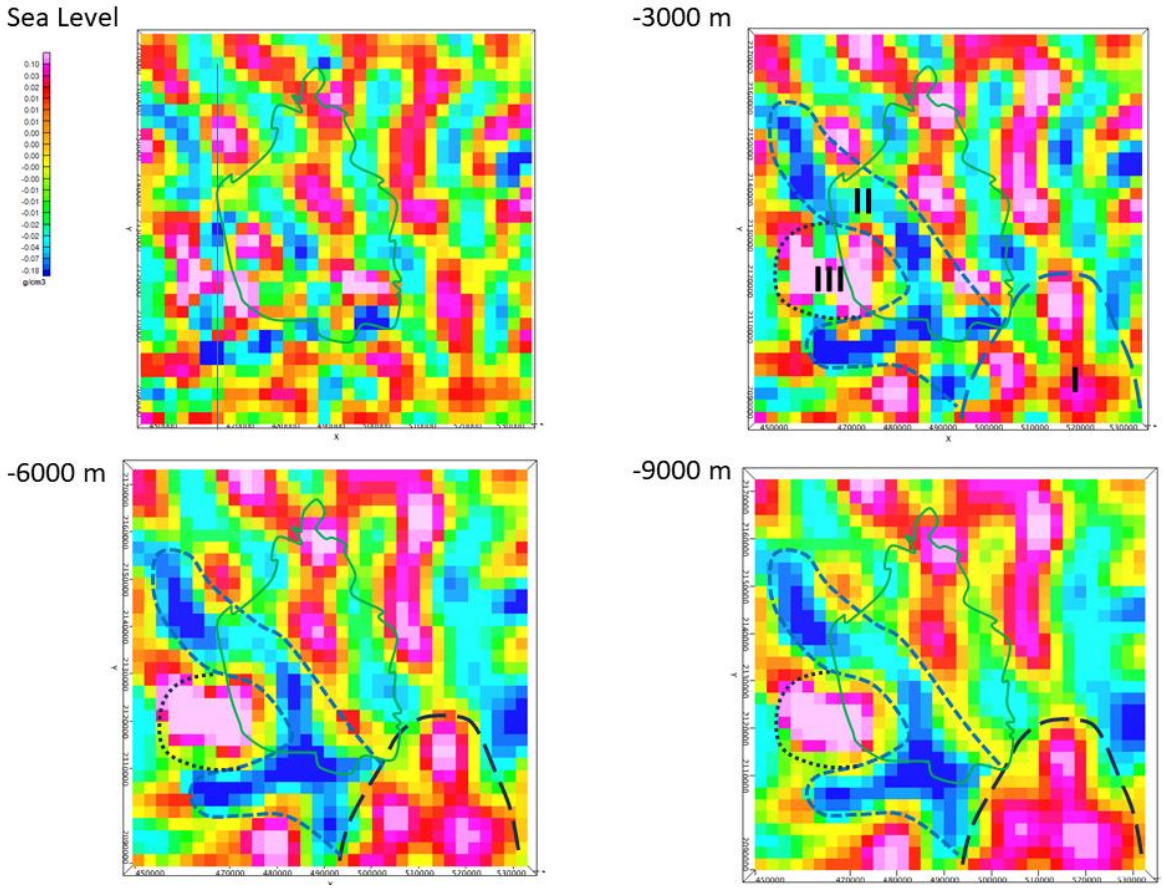


Figure 16: Horizontal density sections at 0, -3, -6, and -9 km depth extracted from the 3D gravity inversion in Figure 6. The contour location of Mexico City is shown in green. Three regions maintain their density pattern with depth: a high-density zone is present from -3 to -9 km (Zone I) on the SE portion of the maps (long dashes), a low-density region persists in the

same depth interval (short dashes, Zone II) with an SE-NW trend, and the high-density region corresponding to the AGA (dots, Zone III).

In Figure 6 of [48], a group of horizontal sections of the crust, from 2 to 50 km depth bsl, at 2-km intervals; they map S-wave velocity in km/sec. Considering that there is a direct correlation between rock density and S-wave velocity, we can perform comparisons between our results and theirs. The depth interval in which comparisons will be made is -10 km since that is the depth reached by our deepest model.

Four horizontal, density distributions at 0, -3, -6, and -9 km bsl, with a resolution of 2500 m, are shown in Figure 16; they are obtained from the inverted volume shown in Figure 6. A high-density trend becomes apparent from -3 km downward (Region I), which most likely continues below the -9 km level. In [48] the authors report a high-velocity region in that section, from 4 to 20 km depth (Vs≈3.95 km/s, Vp≈6.84 km/s), agreeing with our high-density findings in the region where they overlap.

In addition, in [48] Figure 8 the authors report three vertical sections (H-H*, I- I*, and J-J*) that intersect our regions II and III (Figure 16), in which a low-velocity region is mapped down to -20 km; these authors do not specifically discuss this low-velocity zone. In their Figure 6, where horizontal velocity layers are presented, the corresponding low-velocity region appears from 12 to 22 km bsl. We attribute the low velocity in this region to the dominance of the low-density Region II, combined with the low resolution of the velocity maps.

DISCUSSION

Extension in the N-S direction of the region of the basin of Mexico City and its vicinity is confirmed by the behavior of the BA in that direction: from N to S gravity decreases down to the S portion of the city; continuing farther to the S, gravity increases again, up to the region occupied by SCh. In [49] originally identified the development of faults N80-85E in SCh as the result of an active, compressive shearing process in the N45E direction. Subsequently, several studies analyzing a group of over 120 monogenetic cones defined E-W faults [11, 14, 50]; this fault direction is expected from an N-S extension. In [14] the authors also inferred that the Sierra de Santa Catarina alignment originated in a tensional fracture.

Sierra de Las Cruces and Mixhuca fault, on the W portion of the basin, date from the Miocene-Pliocene; the fault is located along a good portion of the boundary between the high- and low-density regions indicated (e.g., Figure 4), ending W of the Saddle Point W. Thus, the fault occurs along the region with the highest gravity gradient in the E-W direction. If the fault originally continued southward, as Sierra de Las Cruces does, its presence was obliterated when Sierra Chichináutzin began to grow at ~700 ka.

CONCLUSIONS

An extensional process in the N-S direction in the Mexico Basin is confirmed by the density distribution, obtained from the Bouguer anomaly map and the corresponding 3D inversions; previous geological reports confirm the extensional nature of this process. A previously unreported gravity anomaly is discovered involving San Miguel and Ajusco volcanoes; it is

shown that it reaches more than 15 km in depth and is formed by two density branches that correspondingly have fed San Miguel and Ajusco volcanoes. We speculate that this anomaly is associated with an extensional episode that occurred before the one giving rise to Sierra Chichináutzin, probably coeval with the formation of Sierra de Las Cruces.

The formation of Sierra Chichináutzin is also linked to the N-S extensional process noting that it occurs immediately S of the region with minimum gravity values in the N-S direction. We can also speculate that at ~700 ka this region might have been the one displaying the minimum gravity values, which eased the dike's intrusion, blocking the drainage of Mexico Basin to the S, and eventually transforming it into the high-gravity, high-density region that we have at present.

The Mixhuca Fault differs in orientation from most of the faults within the Basin of Mexico (Figure 4), yet it conforms well with the trend of the E-W gravity gradient in that region, which is also the limit of Sierra de Las Cruces. If this fault initially continued farther S, as does Sierra de Las Cruces, it was blocked by the AGA and Sierra Chichináutzin structures. Unpublished results unveiled an additional E-W extension that is registered from Malinche volcano in the E, to the approximate location of Mixhuca Fault. Once these developments are confirmed, a re-evaluation of this subject will be done.

The Central Gravity Anomaly displays inverse characteristics as those of the AGA; it shows a marked gravity decrement in the engaged region, which also corresponds to the region where maximum damage has been registered from the 1985 and 2017 earthquakes. This region is crossed on the W by Falla Mixhuca, in a region where this fault departs from the trend it shows to the NW, and where the SW-NE fault in Figure 9 converges with it. A more detailed study of this anomaly will be made elsewhere; here we intend only to focus on its importance.

References

[1] Campillo, M., Bard, P-Y, Nicollin, E., and Sánchez-Sesma, F. (1988). The Mexico earthquake of September 19, 1985-The incident wavefield in Mexico City during the great Michoacán earthquake and its interaction with the deep basin. *Earthquake Spectra*, 4, No. 3, 591-608.

[2] Sánchez-Sesma, F., Chávez-Pérez, S., Suárez, M., Bravo, M.A., and Pérez-Rocha, L.E. (1988). The Mexico earthquake of September 19, 1985-On the seismic response of the valley of Mexico. *Earthquake Spectra*, **4**, 569-589.

[3] Alvarez R., (1986a), Local surface deformations in the September 19, 1985 earthquake in Mexico City. Comunicaciones Técnicas, Serie Naranja, No. 412, 13p, IIMAS-UNAM, México DF. http://biblat.unam.mx/es/revista/comunicaciones-tecnicasserienaranja-investigaciones-instituto-de-investigacionesen-matematicas-aplicadas-y-en-sistemas-unam

[4] Alvarez R., (1986b), Gravimetric definition of underground formations in Mexico City: Relevance for seismic risk. Comunicaciones Técnicas, Serie Naranja, 443, 5p, IIMASUNAM, México DF. http://biblat.unam.mx/es/revista/comunicaciones-tecnicasserie-naranja-investigaciones-instituto-deinvestigaciones-en-matematicas-aplicadasy-en sistemas-unam.

[5] Alvarez R., (1988), Configuración profunda del valle de México: Un estudio gravimétrico. Simp. Generación, Propagación y Efectos de Temblores, Soc. Mex. Fís., Soc. Mex. Mecánica de Suelos, U. Geof. Mex. y Soc. Mex. Ing. Sísmica, 19-31.

[6] Alvarez R., (1990), Structure of the basin of Mexico City and its relation to destruction in the earthquake of 1985, In Geotechnical and Environmental Geophysics, Ed. S. H. Ward, vol. III, 263-280, Soc. Expl. Geophysicists, Tulsa.

[7] Alvarez, R. (2017) Mapping Geologic Interfaces that may alter seismic wave propagation in the Mexico City basin. *Geofísica Internacional*, 56-1: 37-56

[8] Marsal, R. J., y Mazari, M., 1959(1969), El subsuelo de la Ciudad de México: México, D. F., *Univ. Nacional Autónoma de México*, Fac. Ingeniería, 377 p.

[9] Hirt, C., et al., (2013). New ultrahigh-resolution picture of Earth's gravity field. Geophysical Research Letters, 40(16), 4279–4283. https://doi.org/10.1002/grl.5083

[10] Ryan, W.B.F., Carbotte, S.M., Coplan, J., O'Hara, S., Melkonian, A., Arko, R., Weissel, R.A., Ferrini, V., Goodwillie, A., Nitsche, F., Bonczkowski, J. and Zemsky, R. (2009) Global Multi-Resolution Topography (GMRT) Synthesis Data Set. Geochemistry Geophysics Geosystems, 10, Article ID: Q03014.

[11] Arce, JL, Layer, PW, Macías, JL, Morales-Casique, E, García-Palomo, A, Jiménez Domínguez, FJ, Benowitz, J and Vásquez-Serrano, A. (2019): Geology and stratigraphy of the Mexico Basin (Mexico City), central Trans-Mexican Volcanic Belt, Journal of Maps, DOI: 10.1080/17445647.2019.1593251

[12] Fitz-Díaz, E., Hudleston, P., Siebenaller, L., Kirschner, D., Camprubí, A., Tolson, G., & Pi, T. (2011). Insights into fluid flow and water-rock interaction during deformation of carbonate sequences in the Mexican Fold-Thrust Belt. *J. Structural Geology*, 33, 1237–1253.

[13] Alaniz-Álvarez, S. A., & Nieto-Samaniego, A. F. (2005). El sistema de fallas Taxco-San Miguel de Allende y la Faja Volcánica Transmexicana, dos fronteras tectónicas del centro de México activas durante el Cenozoico. Boletín de la Sociedad Geológica Mexicana. Volumen Conmemorativo del Centenario. Grandes Fronteras Tectónicas de México (pp. 65–82). Tomo LVII, núm. 1.

[14] De Cserna, Z., Aranda-Gómez, J. J., & Mitre-Salazar, L. M. (1988). Estructura geológica, gravimetría, sismicidad y relaciones neotectónicas regionales de la cuenca de México. *Boletín del Instituto de Geología*, UNAM, México, 104, 1–71.

[15] García-Palomo, A., Zamorano, J. J., López-Miguel, C., Galván-García, A., Carlos-Valerio, C., Ortega, R., & Macías, J. L. (2008). El arreglo morfoestructural de la Sierra de las Cruces, México central. *Revista Mexicana de Ciencias Geológicas*, 25, 158–178.

[16] Martin del Pozzo, A.L., 1982. Monogenetic volcanism in Sierra Chichinautzin. México.Bull. Volcanol. 45, 9–24.

[17] Martin del Pozzo, A.L., 1989. Geoquímica y paleomagnetismo de la Sierra Chichinautzin. Ph.D. thesis. Universidad Nacional Autónoma de México, México, D.F., 148 p.

[18] Alvarez, R. and Yutsis, V. (2015) Southward Migration of Magmatic Activity in the Colima Volcanic Complex, Mexico: An Ongoing Process. International Journal of Geosciences, 6, 1077-1099. http://dx.doi.org/10.4236/ijg.2015.69085

[19] Gómez-Tuena, A., et al., (2007). Igneous petrogenesis of the Trans-Mexican Volcanic Belt. Special Paper of the Geological Society of America, 422(303), 129–181. https://doi.org/10.1130/2007.2422(05)

[20] Sutter, M., Quintero, O., Lopez, M., Aguirre, G., Farrar, E. (1995) The Acambay graben: active intrarc extension in the Trans-Mexican Volcanic Belt, Mexico. *Tectonics*, 14, 1245-1262.

[21] Márquez, A., Verma, S.P., Anguita, F., Oyarzun, R., Brandle, J.L. (1999a). Tectonics and volcanism of Sierra Chichinautzin: extension at the front of the central Trans-Mexican Volcanic Belt. J. Volcanol. Geotherm. Res. 93, 125 – 150

[22] Mooser, F.M., Nairn, A.E.M., Negendank, J.F.W. (1974). Paleomagnetic investigations of the Tertiary and Quaternary igneous rocks: VIII A paleomagnetic and petrologic study of the volcanics of the Valley of México. *Geol. Rundsch.* **63**, 451–483.

[23] Herrero, E. & Pal, S. (1978). Paleomagnetic study of Sierra de Chichinautzin. *Geofis. Int.* **17**, 167–180.

[24] Márquez, A., and De Ignacio, C. (2002). Mineralogical and geochemical constraints for the origin and evolution of magmas in Sierra Chichinautzin, Central Mexican VolcanicBelt. *Lithos* 62, 35–62.

[25] Singh, S.K., and M. Pardo, (1993) Geometry of the Benioff zone and state of stress in the overriding plate in central Mexico, Geophys. Res. Lett., 20, 1483-1486.

[26] Verma, S.P (1999) Geochemistry of evolved magmas and their relationship with subduction-related mafic volcanism at volcanic front of the Central Mexican Volcanic Belt. *J. Volcanol. Geotheral Res.* **93**, 151-171.

[27] Magee, C et al., (2018). Magma Plumbing Systems: A Geophysical Perspective. Journal of Petrology, 2018, Vol. 59, No. 6, 1217–1251. doi: 10.1093/petrology/egy064

[28] Márquez, A., Oyarzun, R., Doblas, M., Verma, S.P. (1999b). Alkalic (OIB-type) and calc-alkalic volcanism in the Mexican volcanic belt: a case of plume-related magmatism and propagating rifting at an active margin? Geology 27, 51 – 54.

[29] Márquez A., Oyarzun R., de Ignacio, C., Doblas, M. (2001) Southward migration of volcanic activity in the central Mexican Volcanic Belt: asymmetric extension within a two-layer crustal stretching model. J. Volcanol. Geothermal Research, Volume 112, Issues 1–4, December 2001, Pages 175-187. https://doi.org/10.1016/S0377-0273(01)00240-2

[30] Macleod, I.N., Ellis, R.G., 2013. Magnetic vector inversion, a simple approach to the challenge of varying direction of rock magnetization. Australian Society of Exploration Geophysicists, Extended Abstracts 2013, 1–4. Melbourne.

[31] Ellis, R.G., de Wet, B., Macleod, I.N., 2012. Inversion of magnetic data from remanent and induced sources. ASEG Extended Abstracts 2012 (1), 1–4. https://doi.org/ 10.1071/ASEG2012ab117.

[32] Ingram, D.M., Causon, D.M., Mingham, C.G., 2003. Developments in Cartesian cut cell methods. Math. Comput. Simulat. 61 (3–6), 561–572. https://doi.org/10.1016/ S0378-4754(02)00107-6.

[33] Camacho, M. and Alvarez, R. (2021) Geophysical Modeling with Satellite Gravity Data: Eigen-6C4 vs. GGMPlus. *Engineering*, 13, 690-706. https://doi.org/10.4236/eng.2021.1312050

[34] Alvarez, R., Camacho, M. (2023a). Plumbing System of Hunga Tonga Hunga Ha'apai Volcano. J. Earth Sci. 34, 706–716. https://doi.org/10.1007/s12583-022-1792-0

[35] Alvarez, R. & Camacho, M. (2023b). Applying High-Resolution Gravity Analysis to Volcanic Plumbing Systems: The Case of Nevado de Toluca Volcano, Mexico. Transactions on Engineering and Computing Sciences, 11(4). 184-207. https://doi.org/10.14738/tecs.114.15392

[36] Camacho, M. and Alvarez, R. (2024). Delineation of the boundaries of the San Blas Basin, Mexico, merging gravity, magnetic and seismic data. Journal of South American Earth Sciences, 136 (2024) 104818 https://doi.org/10.1016/j.jsames.2024.104818

[37] Osete, M.L., Ruíz-Martínez, V.C., Caballero, M.C., Galindo, C., Urrutia- Fucugauchi, J., Tarling, H.D., (2000). Southward migration of continental volcanic activity in the Sierra de Las Cruces, Mexico: Paleomagnetic and radiometric evidence: *Tectonophysics*, 318, 201-215.

[38] Mejía, V., Böhnel, H., Opdyke, N.D., Ortega-Rivera, M.A., Lee, J.K.W., Aranda-Gómez, J.J., (2005). Paleosecular variation and time-averaged field recorded in late Pliocene-Holocene lava flows from Mexico: Geochemistry Geophysics Geosystems, 6, 1-19.

[39] Arce, J.L., Cruz-Fuentes, D., Ramírez-Luna, A., Herrera-Huerta, I.A., Girón-García, P., (2017), Pómez Bosque de Tlalpan, producto de una erupción de gran magnitud en el margen suroeste de la cuenca de México: Revista Mexicana de Ciencias Geológicas, v. 34, núm. 3, p. 274-288. DOI: http://dx.doi.org/10.22201/cgeo.20072902e.2017.3.485

[40] Arce, J.L., Layer, P.W., Morales-Casique, E., Benowitz, J.A:, Rangel, E., Escolero, O., (2013a), New constraints on the subsurface geology of the Mexico City Basin: The San Lorenzo Tezonco deep well, on the basis of 40Ar/39Ar geochronology and whole-rock chemistry: Journal of Volcanology and Geothermal Research, 266, 34-49.

[41] Siebe, C., (2000). Age and archaeological implications of Xitle volcano, southwestern basin of Mexico-City: J. Volcanol. Geotherm. Res. 104: 45-64.

[42] Siebe, C., Rodríguez-Lara, V., Schaaf, P., Abrams, M., (2004) Radiocarbon ages of Holocene Pelado, Guespalapa, and Chichinautzin scoria cones, south of México City: implications for archaeology and future hazards. *Bull. Volcanol.* **66**, 203–225.

[43] Mooser, F., (1963), Historia tectónica de la Cuenca de México: *Boletin de la Asociación Mexicana de Geólogos Petroleros*, 15, 239-245.

[44] Arce, J.L., Layer, P.W., Lassiter, J., Benowitz, J.A., Macías, J.L., Ramírez- Espinosa, J., (2013b), 40Ar/39Ar dating, geochemistry, and isotopic analyses of the Quaternary Chichinautzin Volcanic Field, south of Mexico City: Implications for timing, effusion rate, and distribution of the volcanism: Bulletin of Volcanology, 75:774, doi: 10.1007/s00445-013-0774-6.

[45] Alvarez, R., Camacho, M., & Rivera-Calderón, E. (2024). The Internal Structure of Paricutin and Tancítaro Volcanos, Mexico, From Rock Density Distributions. Transactions on Engineering and Computing Sciences, 12(2). 50-69. DOI:10.14738/tecs.122.16645.

[46] Chávez-García, F. J., & Quintanar, L. (2010). Velocity structure under the trans-Mexican volcanic belt: Preliminary results using correlation of noise. Geophysical Journal International, 183(2), 1077–1086. https://doi.org/10.1111/j.1365-246X.2010.04780

[47] Iglesias, A., Clayton, R. W., Perez-Campos, X., Singh, S. K., Pacheco, J. F., García, D., & Valdes-Gonzalez, C. (2010). S wave velocity structure below central Mexico using high-resolution surface wave tomography. Journal of Geophysical Research, 115(B6), B06307. https://doi.org/10.1029/2009JB006332

[48] Aguilar-Velazquez, M. J., Perez-Campos, X., & Pita-Sllim, O. (2023). Crustal structure beneath Mexico City from joint inversion of receiver functions and dispersion curves. Journal of Geophysical Research: Solid Earth, 128, e2022JB025047. https://doi.org/10.1029/2022JB025047

[49] Fries, C. Jr. (1960), Geología del Estado de Morelos y de partes adyacentes de México y Guerrero, región central meridional de México: Univ. Nacional Autónoma de México, Inst. Geología, Boletín, 60, 236 p.

[50] Agustín-Flores, J., Siebe, C., Guilbaud, M-N. (2011) Geology and geochemistry of Pelagatos, Cerro del Agua, and Dos Cerros monogenetic volcanoes in the Sierra Chichinautzin Volcanic Field, south of México City. Journal of Volcanology and Geothermal Research 201 (2011) 143–162. doi: 10.1016/j.jvolgeores.2010.08.010